Minerals Engineering 72 (2015) 57–64

Contents lists available at ScienceDirect

Minerals Engineering

journal homepage: www.elsevier.com/locate/mineng

Pyrite oxidation inhibition by organosilane coatings for acid mine drainage control

Yuting Ouyang, Yun Liu *, Runliang Zhu, Fei Ge, Tianyuan Xu, Zan Luo, Libo Liang

Department of Environmental Science and Engineering, Xiangtan University, Hunan Province, Xiangtan 411105, China

ARTICLE INFO

Article history:
Received 28 July 2014
Accepted 13 December 2014
Available online 5 January 2015

Keywords:
Pyrite
Acid mine drainage (AMD)
Inhibition
Organosilane coating

ABSTRACT

By using electrochemical techniques and conventional chemical leaching approach, the potential of organosilane coatings to suppress the pyrite oxidation under acidic conditions was investigated, including γ-mercaptopropyltrimethoxysilane (PropS-SH), γ-aminopropyltrimethoxysilane (APS) and vinyltrimethoxysilane (VTMS). The coated pyrite samples were analyzed by Fourier transforms infrared reflection (FT-IR) spectroscopy and X-ray photoelectron spectrometer (XPS). The results from electrochemical tests have indicated that all the studied coatings could suppress the oxidation of pyrite and the inhibition efficiency should follow the sequence of PropS-SH > VTMS > APS. The results of chemical leaching experiments have showed that pyrite oxidation was decreased by 49.4%, 71.4% and 89.2% (based on Fe release) respectively by using APS, VTMS and PropS-SH coatings. The mechanism of inhibition action could possibly be the formation of a cross-linking network of Si–O–Si and Si–O–Fe bonds on the pyrite surface which could restrain the permeation of aggressive species.

© 2014 Elsevier Ltd. All rights reserved.

1. Introduction

Pyrite (FeS_2) is a common metal sulfide mineral in tailings and valuable mineral raw materials (Peppas et al., 2000). Pyrite is unstable in oxidizing environments. When exposed to liquid water and oxygen, pyrite can undergo rapid weathering (Joeckel et al., 2005). Weathering of pyrite results in the production of sulfuric acid and dissolved ferric ions, which in turn increase the dissolution of pyrite and accelerate the release of toxic metals from coexisting minerals (Jiang et al., 2000), The toxic heavy metals of pyrite leachate could enrich in organisms, on the other hand, it could enter into the human body through food chain and do harm to the health of people (Sánchez-Chardi et al., 2009). These processes lead to the formation of acid mine drainage (AMD) (Akcil and Koldas, 2006; Sheoran and Sheoran, 2006). In addition, fewer studies (Sracek et al., 2004; Strömberg and Banwart, 1999) have documented the higher pyrite content in waste rocks, the faster release of heavy metals on account of acid production. These are the reasons why many researchers have selected pyrite as research subject to study to AMD formation. AMD is often characterized by low pH water with elevated concentrations of iron, sulfates and heavy metals. As a result, AMD is a serious and persistent problem in watersheds with active or abandoned mines.

In the past decades, several post-treatments have been proposed to control AMD (Coulton et al., 2003; Kalin and Caetano Chaves, 2003). The most commonly used treatment method is chemical neutralization using a suitable alkali such as lime, soda ash, caustic soda and magnesium oxide (Caraballo et al., 2009; Mackie and Walsh, 2012). This method works well for the remediation of AMD, however, it has main drawbacks of high cost for large doses of alkaline materials and producing bulky iron-rich sludge as secondary pollutant (Johnson and Hallberg, 2005). These drawbacks limit the use of chemical neutralization on a large scale.

Recently, methods for the source control of AMD by suppressing the oxidation of sulfide minerals have been developed. One such treatment involves the passivation of pyrite, in which a thin organic or inorganic protective coating is formed on the surface of pyrite to prevent its contact with the air, water and other oxidants (Lu et al., 2001). To date, numerous passivation agents have been reported, including silicate (Kargbo and Chatterjee, 2005), phosphate (Kargbo et al., 2004; Zhang et al., 2003), 8-hydroxyquinoline (Lan et al., 2002), triethylenetetramine (TETA) (Chen et al., 2006; Liu et al., 2013) or sodium triethylenetetramine-bisdithiocarbamate (DTC-TETA) (Shu et al., 2013) that create ferric silicate, ferric phosphate or organic iron complexes on the surface of pyrite and subsequently reduce the rate of pyrite oxidation. Unfortunately, each of these passivation agents has their own disadvantages. For example, the formation of phosphate, silicate and 8-hydroxyquinoline coatings require initial surface oxidation using

* Corresponding author. Tel./fax: +86 731 58292231.
E-mail addresses: oyt0225@126.com (Y. Ouyang), liuyunscut@163.com (Y. Liu).

http://dx.doi.org/10.1016/j.mineng.2014.12.020
0892-6875/© 2014 Elsevier Ltd. All rights reserved.

hydrogen peroxide (H_2O_2), which is difficult to handle in real application. Other passivation agents, such as triethylenetetramine and sodium triethylenetetramine-bisdithiocarbamate (DTC-TETA), are toxic to the environment. Thus, it is necessary to seek more environmentally friendly alternatives. Organosilanes, a kind of harmless and environmentally friendly materials, have been widely applied in anticorrosion field of metals and their alloys, which are identified as excellent coupling agents owing to generating Me–O–Si bond on the metal substrate and simultaneously creating a crosslinked Si–O–Si network (Zhou et al., 2013; Zhu and van Ooij, 2003) to protect metals efficiently against corrosion. However, knowledge on the application of organosilanes for suppression of pyrite oxidation is scarce. Additionally, most of the protection effects of coatings on pyrite have been evaluated by chemical methods. Pyrite dissolution is usually interpreted as electrochemical behavior (Ogunsola and Osseo-Asare, 1987), but only a limited number of investigations on pyrite passivation by electrochemical methods have been reported.

In the present work, three kinds of organic silanes with different functional groups, including γ-mercaptopropyltrimethoxysilane (PropS-SH), γ-aminopropyltrimethoxysilane (APS) and vinyltrimethoxysilane (VTMS), were selected as coating agents to suppress oxidation of pyrite for remediation of AMD. A preliminary assessment of inhibitory efficiencies for pyrite coatings was provided by using electrochemical tests, such as cyclic voltammetry (CV), Tafel polarization and electrochemical impedance spectroscopy (EIS). Traditional chemical leaching tests were also used to further verify the effects of organic silanes on the rate of pyrite oxidation. Furthermore, the chemical characteristics of these organic silane films were analyzed with X-ray photoelectron spectrometer (XPS) and Fourier transform infrared reflection (FT-IR) spectroscopy. The aim of this study is focusing on seeking an effective passivant to suppress oxidation of pyrite. There is a need for more systematic studies on the application of selected passivant to sulfide mineral wastes and the simplification of coating procedure in the future research.

2. Experimental

2.1. Materials preparation

The pyrite sample used in the study was purchased from ChangSha Mineral market. The chemical composition analyzed by X-ray fluorescence (Table 1) shows that the purity of FeS_2 is 99.56% and the main impurity is Al_2O_3. Pyrite samples with fine crystallization were cut into cubes with side length of 1 cm and polished sequentially into mirror-like surface with waterproof abrasive papers (grit size 600–2000). After polishing, the pyrite cubes were rinsed with ultrapure water and acetone to remove any species that may have remained on the electrode surface. The remaining samples were ground with an agate mortar and then sieved to isolate particles with diameter less than 75 μm. All samples prepared were stored in a vacuum desiccator at room temperature. All reagents used in the experiment were of analytical grade and ultrapure water was used to prepare solutions.

Table 1
Chemical composition of the studied pyrite sample.

Compound	Mass (%)
FeS_2	99.56
Al_2O_3	0.35
NiO	0.08
P_2O_5	0.01

2.2. Coating processing

The silanol solutions were prepared by adding organosilane compound (PropS-SH, APS or VTMS) to a mixture of ultrapure water and ethanol. The volume ratio of organosilane/ultrapure water/ethanol was 1:1:8. Hydrochloric acid was used to adjust the pH to 4. The silanol solutions were stirred for 1 h at 40 °C to make it workable. Then pyrite cubes or pyrite powders prepared previously were dissolved in the silanol solutions and then the solutions were kept stirring for 2 h at 50 °C after adjusting the pH to 9 with 0.5 M ammonium hydroxide. The coated samples were separated from solutions and dried at 100 °C for 12 h.

2.3. Anticorrosive effect experiments

2.3.1. Electrochemical test

A conventional three-electrode system was adopted in the electrochemical experiments with pyrite electrode as working electrode, Pt foil (15 mm × 15 mm) as counter electrode and saturated calomel electrode (SCE) with a Luggin's capillary as reference electrode. Pyrite electrode was prepared as follows: each coated or uncoated pyrite cube was electrically connected to a copper wire with conductive silver adhesive and mounted in epoxy resin with one side exposed.

The electrochemical measurements were performed at CHI 660 Electrochemical Workstation at room temperature and all potentials quoted in this paper were referenced to the SCE. The electrolyte was 0.2 M sodium sulfate solution with pH of 2, which was adjusted by sulfuric acid. Cyclic voltammetry tests were conducted at a sweep rate of 100 mV/s and the scan ranged from −0.7 V/SCE to +0.7 V/SCE. Tafel polarization curves were recorded over the range of OCP ± 0.2 V/SCE at a scan rate of 1 mV/s. The EIS tests were measured at open circuit potential over the frequency range of 10^5 Hz–0.1 Hz with the AC signal amplitude of 10 mV. The EIS data were analyzed by using ZSimpWin 3.00 software.

2.3.2. Chemical leaching test

Chemical leaching test was operated by adding 1.0 g sample of coated and uncoated pyrite into 120 ml 3 wt% hydrogen peroxide solution with the natural pH of 3.1. The mixture was placed in vapor-bathing constant temperature vibrator with rotating speed of 150 rpm and the constant temperature is 25 °C. A 5-ml sample of leaching solution was collected at the following time: 0.5, 1, 2, 4, 6, 8, 10, 12, 24, 36, 48 and 60 h. Prior to analysis, the collected leaching solution was filtered through a 0.22 μm pore size filter to get rid of impurities. The pH value, total Fe and SO_4^{2-} concentration of the solution were measured. The pH value of the leaching solution was determined by a waterproof hand-held pH/mV meter (Eutech instruments pH 310, USA). Total Fe of the leaching solution was analyzed by o-phenanthroline spectrophotography (UV-752N, Shanghai Analytical Instrument Co. Ltd., China) and the absorbance reading was taken at 510 nm. SO_4^{2-} concentration of the leachate was determined by the baryta yellow spectrophotometric method. All chemical leaching tests were repeated 3 times to ensure repeatability and accuracy of the measurements.

2.4. Analytical methods

FT-IR Spectrometer (Nicolet 380, USA) was applied to characterize the chemical structure of the coated pyrite samples. A measured amount of organosilane coatings or pyrite samples were mixed with KBr powder and pressed into pellets at the pressure of 8 MPa. The FT-IR spectra were collected in a transmittance mode from 4000 to 400 cm^{-1}.

The surface compositions of coated and uncoated pyrite were analyzed by X-ray photoelectron spectrometer (XPS). The XPS

spectra were obtained by using the Al Kα source (1486.8 eV) with a Thermo Scientific Escalab 250 analyzer.

3. Results and discussion

3.1. Electrochemical tests

The cyclic voltammetric curves of pyrite electrodes with and without coating treatment are shown in Fig. 1. In the curve of uncoated pyrite electrode, three anodic current peaks and a cathodic current peak can be observed, which is in agreement with those reported by Giannetti (Giannetti et al., 2001). The anodic current peak at around −0.1 V is attributed to the oxidation of H_2S which is formed at lower potentials. As potential increases approximately to 0.2 V, The oxidation of FeS_2 occurs and element sulfur S^0 is formed, illustrated by the following reactions:

$$FeS_2 \rightarrow Fe^{2+} + 2S^0 + 2e^- \quad (1)$$

When the potential is larger than 0.6 V, the dissolution of element sulfur is expected to occur, contributing to the appearance of the anodic current peak between 0.6 and 0.7 V. During reverse scanning process of cathode, a reduction peak between −0.2 and −0.65 V is observed. It can be interpreted as two possible reactions: (a) the reduction of FeS_2 (s) to form FeS (s) and H_2S, and (b) the reduction of S which is formed electrochemically during the oxidation scan. These reactions can be represented by:

$$FeS_2 + 2H^+ + 2e^- \rightarrow FeS + H_2S \quad (2)$$

$$S^0 + 2H^+ + 2e^- \rightarrow H_2S \quad (3)$$

Comparing the CV curves of uncoated and coated pyrite electrodes, the oxidation and reduction peaks are significantly reduced with organosilanes modification. These results suggest that the protective layers of silane coatings have been formed on the surface of substrate, inhibiting the dissolution of pyrite. The inhibition efficiency of the three kinds of organosilanes on pyrite are compared, following the order of PropS-SH > VTMS > APS. When PropS-SH is adopted in the coating treatment, the anodic and cathodic current peaks almost cannot be detected, suggesting silane molecules with thiolate have built a very corrosion resistant coating on pyrite. These results may be ascribed to the hydrophobicity difference among the studied organosilane coatings. As confirmed by previous researches (Fan et al., 2011; Olsen, 2001), PropS-SH film has a better hydrophobicity than VTMS film, while APS film exhibits the lowest hydrophobicity.

Fig. 2 presents Tafel polarization curves of bare pyrite and coated pyrite electrodes with various organosilane agents in 0.2 M Na_2SO_4 solution (pH = 2). The corrosion current densities (I_{corr}) of different electrodes could be obtained by the Tafel extrapolation method, which are listed in Table 2. The lower polarization current the electrode is, the better corrosion resistance it possesses (Zhang et al., 2008). The value of the I_{corr} is 1.801 μA cm^{-2} for bare pyrite electrode, and that for APS, VTMS and PropS-SH coated pyrite is 0.716, 0.357, 0.090 μA cm^{-2}, respectively. These decreases in I_{corr} show that all the coatings inhibit the oxidation of pyrite. Moreover, the corrosion current density corresponding to the PropS-SH coated pyrite decreases much more than that of APS and VTMS coated pyrite. These results corroborate the idea that PropS-SH coating has much better inhibiting efficiency compared with APS and VTMS.

Fig. 3 compares the impedance spectra (Nyquist plots) of bare and coated pyrite electrodes, obtained in the solution of 0.2 M Na_2SO_4 (pH = 2) at room temperature. It can be seen that the impedance spectra exhibit a depressed capacitive loop, whose diameter increases obviously when pyrite is coated with APS, VTMS and PropS-SH. It indicates that the corrosion resistance of pyrite has been enhanced significantly and the electrode surface has gotten more protection.

The impedance data could be explained by using the equivalent circuit $R_s(Q_1(R_{ct}(Q_2R_f)))$ illustrated in Fig. 4. In this circuit, R_s represents the solution resistance; R_{ct} is the charge transfer resistance reflecting the anticorrosion capability of working electrode; R_f is the resistance of films (corrosion products and/or inhibitor film) formed on the pyrite surface; Constant phase element Q_1 is the diffusion impedance component; and Q_2 represents the diffusion impedance component in which the membrane capacitance is associated with the dielectric nature of surface film. This approach has been used to characterize the corrosion of copper (Li et al., 2011) and has allowed us to obtain a good superposition with the experimental data.

The fitted equivalent circuit parameters are listed in Table 3. It shows that the values of the film resistance R_f has increased after the electrode surface is covered by each organosilane films, suggesting a protective adsorption film of the studied compounds is well formed on the pyrite surface. Generally, the corrosion resistant performance of the coating could be implied by R_{ct} and higher

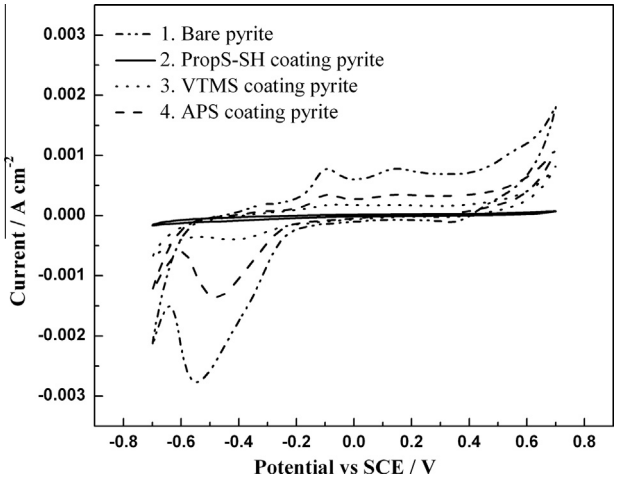

Fig. 1. Cyclic voltammetry curves of bare and coated pyrite electrodes in 0.2 M Na_2SO_4 solution (pH = 2) at room temperature.

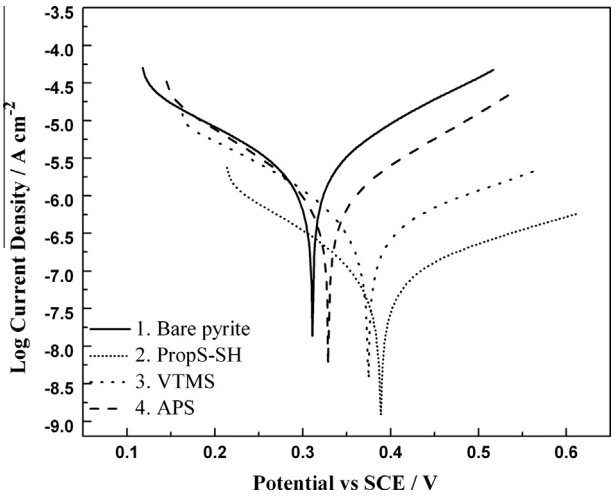

Fig. 2. Tafel polarization curves of bare and coated pyrite electrodes in 0.2 M Na_2SO_4 solution (pH = 2) at room temperature.

Table 2
Tafel polarization parameters for bare pyrite and coated pyrite electrodes with various organosilane agents.

Organosilane agents	E_{corr} (mV/SCE)	β_c (decade V^{-1})	β_a (decade V^{-1})	I_{corr} ($\mu A\ cm^{-2}$)
Bare pyrite	311	8.18	7.23	1.801
APS	329	8.13	6.97	0.716
VTMS	375	8.77	4.86	0.357
PropS-SH	389	7.64	4.70	0.090

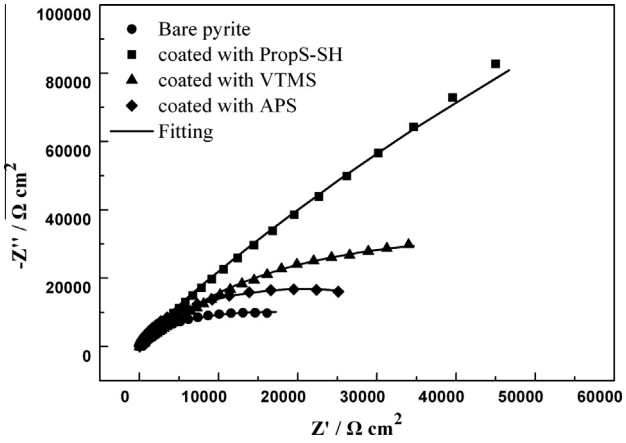

Fig. 3. Nyquist impedance plots of bare and coated pyrite electrodes in 0.2 M Na_2SO_4 solution (pH = 2) at room temperature.

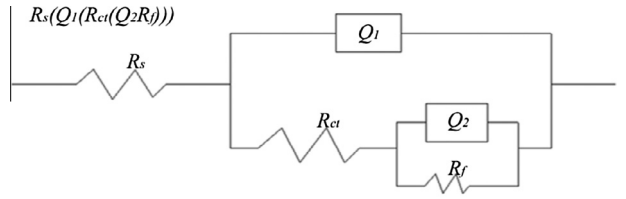

Fig. 4. Equivalent circuit proposed for fitting impedance spectra obtained with bare and coated pyrite electrodes.

R_{ct} value indicates better resistance behaviors (Peng et al., 2011). As shown in Table 3, the R_{ct} of APS, VTMS and PropS-SH coated pyrite are 1.73×10^4, 2.51×10^4 and $10.85 \times 10^4\ \Omega\ cm^2$, respectively, which are much higher than that of bare pyrite (i.e., $0.41 \times 10^4\ \Omega\ cm^2$). Specifically, the PropS-SH coating exhibits the highest charge resistance among the studied coatings. It is consistent with the results obtained from Tafel test.

3.2. Chemical leaching test

The ability of the studied organosilane coatings to suppress chemical oxidation of pyrite was evaluated in a chemical leaching test, using hydrogen peroxide (H_2O_2) as an oxidation agent, with the results shown in Figs. 5 and 6. In the leaching test, total iron and SO_4^{2-} are selected as indicators to evaluate the degree of pyrite oxidation. The concentrations of total Fe and SO_4^{2-} released into solution from bare pyrite after 60 h are 1.29 and 12.03 mM (as shown in Fig. 5). In contrast, the total Fe released from pyrite coated with PropS-SH, VTMS and APS is decreased by 89.2%, 71.4% and 49.4%, respectively, and the SO_4^{2-} concentration in corresponding solution is reduced by 89.6%, 69.1% and 45.1%, respectively. All organosilane coatings in the test have certain protective effects from pyrite oxidation. Obviously, the PropS-SH coating is superior to the other two organosilane coatings.

Fig. 6 shows the influence of pyrite oxidation on the pH value of solution. The decrease of pH values is observed in each treatment, which is ascribed to the release of H^+ ions derived from pyrite oxidation. By comparison, the pH in uncoated pyrite treatment decreases in the fastest way, declining from 3.1 to 1.19. While the pH decrease of APS, VTMS and PropS-SH coated pyrite treatments is from 3.1 to 1.88, 2.26 and 2.57, respectively, indicating that the PropS-SH coating is highly effective in suppressing oxidation of pyrite. The APS and VTMS coatings also can suppress pyrite oxidation but in a less extent. The good fitness between the experimental results of electrochemical measurements and chemical oxidation test indicates both techniques have high reliability in evaluating the performance of samples.

3.3. Structure characteristic of coated pyrite samples

3.3.1. FT-IR analysis

In order to investigate the chemical bonds on the surface of organosilane-coated pyrite, the three kinds of studied organosilane coatings and the corresponding coated pyrite samples were analyzed by FT-IR spectroscopy, which are presented in Fig. 7. In the spectra of APS coating and APS-coated pyrite (Fig. 7a), the peaks at 3422, 3435, 1651, 1616 cm^{-1} can be attributed to O–H bonds while the adsorption bonds at 787, 798, 1036, 1048, 1088, 1146 cm^{-1} are assigned to Si–O–Si asymmetric stretching vibration bonds (Lee et al., 2002). The occurrence of Si–O–Si bonds confirms the formation of a network structure in APS coating. Furthermore, according to Jeong et al. (2000) and Ren et al. (2011), peaks located at 3034, 2976, 1507, 1415, 1412, 697 and 680 cm^{-1} are attributed to C–H stretching and bending, while the peaks at 1274 and 1228 cm^{-1} belong to Si–C stretching in Si–CH_2 bonds. Similarly, characteristic absorption peaks corresponding to O–H, Si–O–Si, C–H and Si–C bonds can also be found in the FT-IR spectra of VTMS coating, VTMS-coated pyrite (Fig. 7b), PropS-SH coating and PropS-SH coated pyrite (Fig. 7c). From the spectra of PropS-SH coating and PropS-SH coated pyrite, we can also find

Table 3
Estimated parameters from the experimental results for the bare and coated pyrite electrodes shown in Fig. 3 by fitting to equivalent circuit shown in Fig. 4.

Organosilane agents	R_s ($\Omega\ cm^2$)	Q_1 Y_1 (10^{-4})		R_{ct} ($\Omega\ cm^2\ 10^4$)	Q_2 Y_2 (10^{-5})		R_f ($\Omega\ cm^2\ 10^4$)
		S ($s^n\ cm^{-2}$)	n		S ($s^n\ cm^{-2}$)	n	
Bare pyrite	21.62	1.89	0.97	0.41	11.35	0.65	2.43
APS	19.23	1.72	0.95	1.73	7.74	0.69	2.95
VTMS	21.97	0.49	0.78	2.51	2.95	0.73	7.28
PropS-SH	19.98	0.01	0.77	10.85	1.71	0.74	68.68

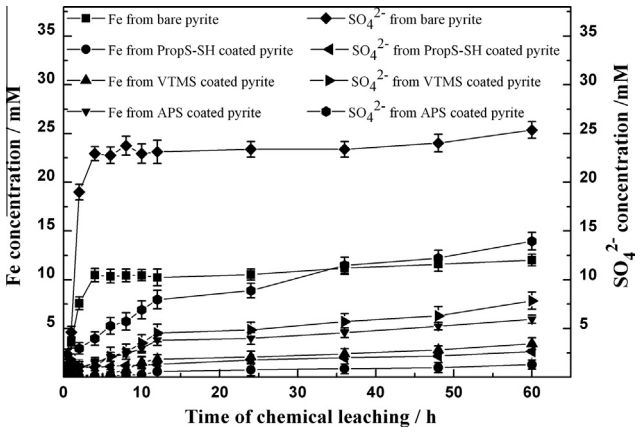

Fig. 5. Release of Fe and SO_4^{2-} as a function of time for bare and coated pyrite samples in the chemical leaching test.

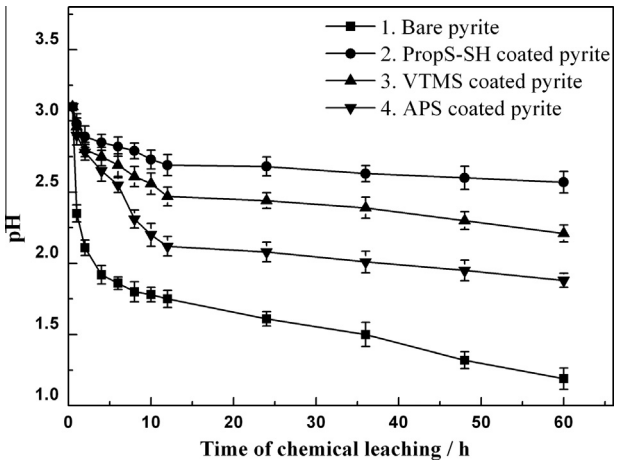

Fig. 6. The solution pH at different time in the chemical leaching test.

the S–H stretching vibration adsorption peaks at 2550 and 2553 cm^{-1}.

Besides, the absorption peak sat 937, 915, 578, 580 and 584 cm^{-1} are observed in APS-coated pyrite, VTMS-coated pyrite and PropS-SH coated pyrite. These peaks are due to the Fe–O stretching of Si–O–Fe bonds (Chanéac et al., 1996; Schwertmann and Thalmann, 1976), indicating that Si–OH groups have reacted with iron oxyhydroxide on the surface of pyrite. Chemical adhesion of organosilane coatings on the surface of pyrite can be attributed to Si–O–Fe bonds.

3.3.2. XPS measurements

The representative spectra for Fe 2p, O 1s and Si 2p are exhibited in Fig. 8 by XPS surveying of bare pyrite and coated with APS, VTMS and PropS-SH. Four samples, including uncoated pyrite, APS coated pyrite, VTMS coated pyrite and PropS-SH coated pyrite, were characterized by XPS in order to identify the chemical changes at pyrite surface before and after coated. Fe 2p spectra of the four samples are illustrated in Fig. 8(a)–(d). The peaks centered at 706.70 and 720.10 eV are attributed to pyritic iron(II), while the peak at 709.23 eV is in accord with iron oxyhydroxide (Descostes et al., 2000). A new peak at around 711.30 eV is observed from the coated pyrite samples, corresponding to iron/silicon dioxide (Gettings and Kinloch, 1977). The occurrence of the peak confirms the formation of Fe–O–Si bonds in organosilane coated pyrite, which is in agreement with the analysis of FT-IR

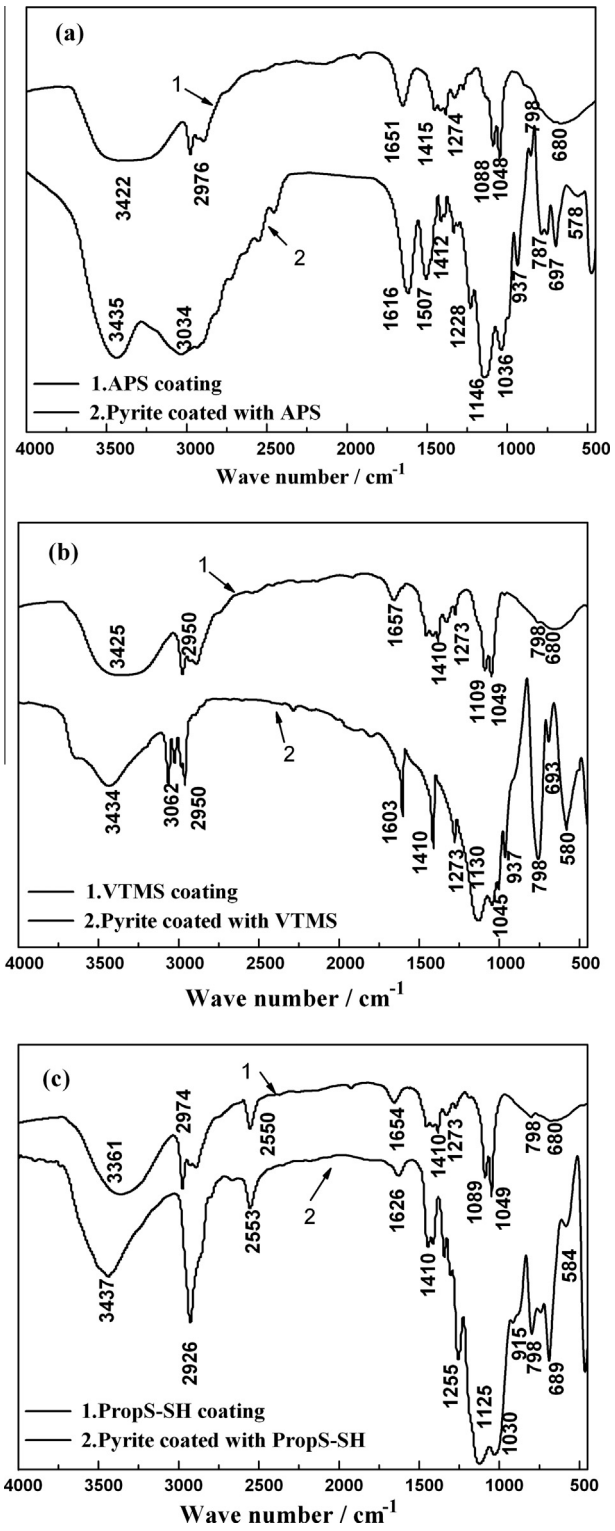

Fig. 7. FT-IR spectra of (a) APS coating and APS-coated pyrite; (b) VTMS coating and VTMS-coated pyrite; (c) PropS-SH coating and PropS-SH coated pyrite.

spectra. As to O 1s spectrum of the four samples (Fig. 8(e)–(h)), the peaks observed around 533.30, 531.90 and 530.00 eV belong to adsorbed water, iron oxyhydroxide and iron oxides, respectively. Moreover, the peaks around 532.01 and 532.50 eV are observed in spectra of organosilane coated pyrite and assigned to silicon dioxide and iron/silicon dioxide, respectively. These results indicate that the Si–O–Si bonds have been formed on the surface of coated

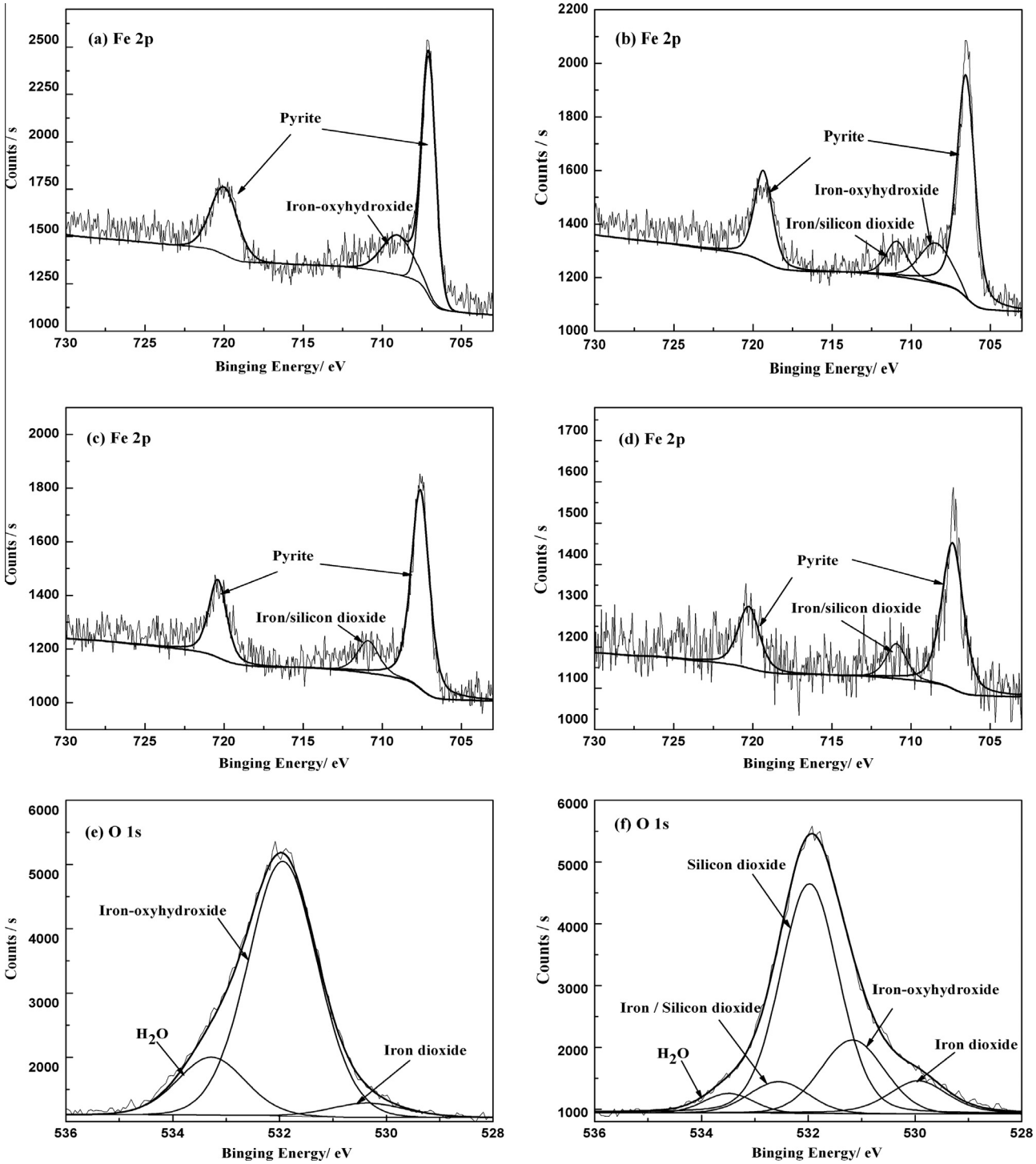

Fig. 8. XPS spectra of bare pyrite, APS coated pyrite, VTMS coated pyrite and PropS-SH coated pyrite. (a) Fe 2p peak of bare pyrite; (b) Fe 2p peak of APS coated pyrite; (c) Fe 2p peak of VTMS coated pyrite; (d) Fe 2p peak of PropS-SH coated pyrite; (e) O 1s peak of bare pyrite; (f) O 1s peak of APS coated pyrite; (g) O 1s peak of VTMS coated pyrite; (h) O 1s peak of PropS-SH coated pyrite; (i) Si 2p peak of APS coated pyrite; (j) Si 2p peak of VTMS coated pyrite; (k) Si 2p peak of PropS-SH coated pyrite.

pyrite. Silicon was not detected on the uncoated pyrite but could be found in all the organosilane coated pyrite samples. It is confirmed that organosilane coatings have existed on the surface of coated pyrite. The Si 2p spectra of the coated pyrite samples are displayed in Fig. 8(i)–(k)). Three kinds of binding energies for the Si 2p peak can be observed. The peaks around 102.10 and 102.80 eV are attributed to silicon dioxide and silicon carbide (Kallury et al., 1991), respectively. While the peak recorded at 103.50 eV is in accord with iron/silicon dioxide (Paparazzo, 1987).

From the analysis of the FT-IR and XPS spectra, it can be concluded that the mechanism of studied organosilane coatings on pyrite oxidation suppression involves the formation of Si–O–Fe bonds at the coating/pyrite interface and Si–O–Si cross-linking network surrounding pyrite, thus resulting in an effective barrier from aggressive species.

The paper has provided a theoretical research on three kinds of organosilane-based coatings to reduce the oxidation of pyrite in the laboratory conditions, and this method is suitable for

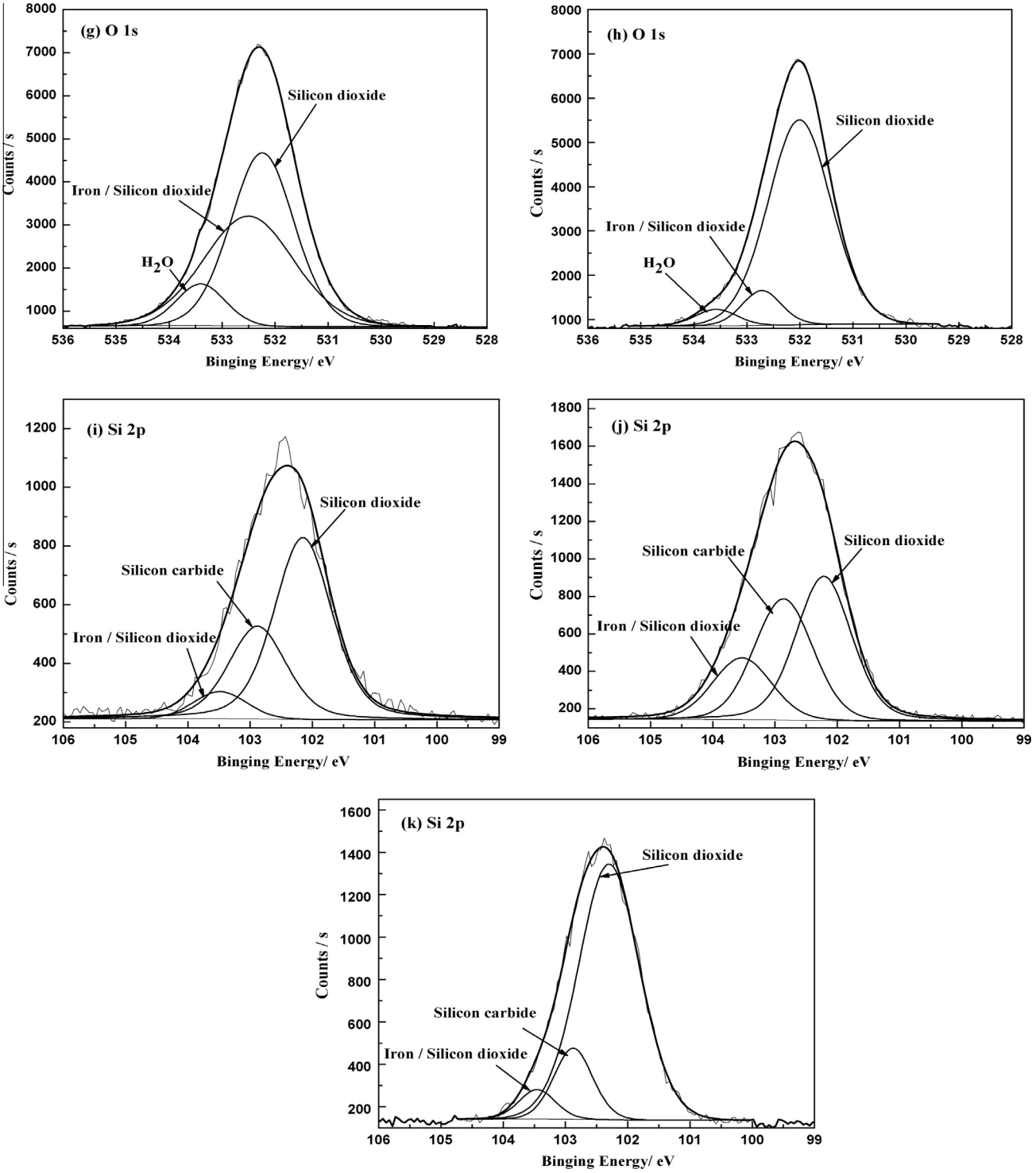

Fig. 8 (*continued*)

high-grade sulfide tailings or waste rock. As to scale the treatment up, further studies to seek a more moderate reaction condition of coating procedure are needed so that the passivant can be prepared on site. Hence, the optimization of organosilane coatings on pyrite to reach the application requirements is our main task in the next work. Additionally, we consider fixing the screened passivant into clay mineral at a proper ratio to make a solid passivation material. Thus, using the solid passivation material to cover on the surface of tailings or waste rock, it can not only suppress pyrite oxidation but also absorb the heavy metals of leachate even if pyrite oxidation occurred.

4. Conclusions

The feasibility of using environmental friendly organosilane-based coatings to reduce the oxidation of pyrite has been demonstrated in this study. The results have indicated that APS,

VTMS and PropS-SH could suppress not only the electrochemical but also the chemical oxidation of pyrite. The inhibitive action of the studied organosilane coatings can be explained by the formation of a dense network of Si–O–Si and Fe–O–Si covalent bonds on the pyrite surface which limited permeation of aggressive species. Among tested coatings, the most effective inhibitor of pyrite was PropS-SH and followed by VTMS, APS. It is better hydrophobicity and flexibility that makes PropS-SH more effective than the other two coatings. However, additional studies are required to simplify the coating procedure and improve stability or durability of organosilane coating on pyrite and tailings in real AMD environments.

Acknowledgments

The authors gratefully acknowledge the financial support of National Natural Science Foundation of China (No. 21207111), Research Foundation of Education Bureau of Hunan Province, China (No. 14B177).

References

Akcil, A., Koldas, S., 2006. Acid Mine Drainage (AMD): causes, treatment and case studies. J. Clean. Prod. 14 (12), 1139–1145.
Caraballo, M.A., Rötting, T.S., Macías, F., Nieto, J.M., Ayora, C., 2009. Field multi-step limestone and MgO passive system to treat acid mine drainage with high metal concentrations. Appl. Geochem. 24 (12), 2301–2311.
Chanéac, C., Tronc, E., Jolivet, J.P., 1996. Magnetic iron oxide–silica nanocomposites. Synthesis and characterization. J. Mater. Chem. 6 (12), 1905–1911.
Chen, Y.W., Li, Y., Cai, M.F., Belzile, N., Dang, Z., 2006. Preventing oxidation of iron sulfide minerals by polyethylene polyamines. Miner. Eng. 19 (1), 19–27.
Coulton, R., Bullen, C., Hallett, C., 2003. The design and optimisation of active mine water treatment plants. Land Contam. Reclam. 11 (2), 273–280.
Descostes, M., Mercier, F., Thromat, N., Beaucaire, C., Gautier-Soyer, M., 2000. Use of XPS in the determination of chemical environment and oxidation state of iron and sulfur samples: constitution of a data basis in binding energies for Fe and S reference compounds and applications to the evidence of surface species of an oxidized pyrite in a carbonate medium. Appl. Surf. Sci. 165 (4), 288–302.
Fan, H., Li, S., Zhao, Z., Wang, H., Shi, Z., Zhang, L., 2011. Inhibition of brass corrosion in sodium chloride solutions by self-assembled silane films. Corros. Sci. 53 (12), 4273–4281.
Gettings, M., Kinloch, A., 1977. Surface analysis of polysiloxane/metal oxide interfaces. J. Mater. Sci. 12 (12), 2511–2518.
Giannetti, B., Bonilla, S., Zinola, C., Rabóczkay, T., 2001. A study of the main oxidation products of natural pyrite by voltammetric and photoelectrochemical responses. Hydrometallurgy 60 (1), 41–53.
Jeong, A.Y., Koo, S.M., Kim, D.P., 2000. Characterization of hydrophobic SiO_2 powders prepared by surface modification on wet gel. J. Sol-Gel. Sci. Technol. 19 (1–3), 483–487.
Jiang, C., Wang, X., Parekh, B., 2000. Effect of sodium oleate on inhibiting pyrite oxidation. Int. J. Miner. Process. 58 (1), 305–318.
Joeckel, R., Ang Clement, B., VanFleet Bates, L., 2005. Sulfate-mineral crusts from pyrite weathering and acid rock drainage in the Dakota Formation and Graneros Shale, Jefferson County, Nebraska. Chem. Geol. 215 (1), 433–452.
Johnson, D.B., Hallberg, K.B., 2005. Acid mine drainage remediation options: a review. Sci. Total Environ. 338 (1), 3–14.
Kalin, M., Caetano Chaves, W., 2003. Acid reduction using microbiology: treating AMD effluent emerging from an abandoned mine portal. Hydrometallurgy 71 (1), 217–225.
Kallury, K.M., Debono, R.F., Krull, U.J., Thompson, M., 1991. Covalent binding of amino, carboxy, and nitro-substituted aminopropyltriethoxysilanes to oxidized silicon surfaces and their interaction with octadecanamine and octadecanoic acid studied by X-ray photoelectron spectroscopy and ellipsometry. J. Adhes. Sci. Technol. 5 (10), 801–814.
Kargbo, D.M., Chatterjee, S., 2005. Stability of silicate coatings on pyrite surfaces in a low pH environment. J. Environ. Eng. 131 (9), 1340–1349.
Kargbo, D.M., Atallah, G., Chatterjee, S., 2004. Inhibition of pyrite oxidation by a phospholipid in the presence of silicate. Environ. Sci. Technol. 38 (12), 3432–3441.
Lan, Y., Huang, X., Deng, B., 2002. Suppression of pyrite oxidation by iron 8-hydroxyquinoline. Arch. Environ. Contam. Toxicol. 43 (2), 168–174.
Lee, C., Kim, G., Hyun, S., 2002. Synthesis of silica aerogels from waterglass via new modified ambient drying. J. Mater. Sci. 37 (11), 2237–2241.
Li, W., Hu, L., Zhang, S., Hou, B., 2011. Effects of two fungicides on the corrosion resistance of copper in 3.5% NaCl solution under various conditions. Corros. Sci. 53 (2), 735–745.
Liu, Y., Dang, Z., Xu, Y., Xu, T., 2013. Pyrite passivation by triethylenetetramine: an electrochemical study. J. Anal. Methods Chem..
Lu, L., Wang, R., Xue, J., Lu, J., 2001. The surface reaction of sulfide minerals and its application to the study of mine environment. Acta Petrol. Mineral. 20 (4), 387–394.
Mackie, A.L., Walsh, M.E., 2012. Bench-scale study of active mine water treatment using cement kiln dust (CKD) as a neutralization agent. Water Res. 46 (2), 327–334.
Ogunsola, O.M., Osseo-Asare, K., 1987. The electrochemical behaviour of coal pyrite: 2. Effects of coal oxidation products. Fuel 66 (4), 467–472.
Olsen, B.A., 2001. Hydrophilic interaction chromatography using amino and silica columns for the determination of polar pharmaceuticals and impurities. J. Chromatogr. A 913 (1), 113–122.
Paparazzo, E., 1987. X-ray photo-emission and Auger spectra of damage induced by Ar^+ etching at SiO_2 surfaces. J. Phys. D Appl. Phys. 20 (8), 1091.
Peng, C.W., Hsu, C.H., Lin, K.H., Li, P.L., Hsieh, M.F., Wei, Y., Yeh, J.M., Yu, Y.H., 2011. Electrochemical corrosion protection studies of aniline-capped aniline trimer-based electroactive polyurethane coatings. Electrochim. Acta 58, 614–620.
Peppas, A., Komnitsas, K., Halikia, I., 2000. Use of organic covers for acid mine drainage control. Miner. Eng. 13 (5), 563–574.
Ren, X.M., Wei, C.P., Cheng, G., 2011. Synthesis, photoluminescence and energy transfer of two novel Tb (III) ternary complexes. Adv. Mater. Res. 216, 502–505.
Sánchez-Chardi, A., Ribeiro, C.A.O., Nadal, J., 2009. Metals in liver and kidneys and the effects of chronic exposure to pyrite mine pollution in the shrew Crocidura russula inhabiting the protected wetland of Doñana. Chemosphere 76 (3), 387–394.
Schwertmann, U., Thalmann, H., 1976. The influence of [Fe (II)], [Si], and pH on the formation of lepidocrocite and ferrihydrite during oxidation of aqueous $FeCl_2$ solutions. Clay Miner. 11 (3), 189–200.
Sheoran, A., Sheoran, V., 2006. Heavy metal removal mechanism of acid mine drainage in wetlands: a critical review. Miner. Eng. 19 (2), 105–116.
Shu, X., Dang, Z., Zhang, Q., Yi, X., Lu, G., Guo, C., Yang, C., 2013. Passivation of metal-sulfide tailings by covalent coating. Miner. Eng. 42, 36–42.
Sracek, O., Choquette, M., Gélinas, P., Lefebvre, R., Nicholson, R.V., 2004. Geochemical characterization of acid mine drainage from a waste rock pile, Mine Doyon, Quebec, Canada. J. Contam. Hydrol. 69 (1), 45–71.
Strömberg, B., Banwart, S., 1999. Weathering kinetics of waste rock from the Aitik copper mine, Sweden: scale dependent rate factors and pH controls in large column experiments. J. Contam. Hydrol. 39 (1), 59–89.
Zhang, X., Borda, M.J., Schoonen, M.A., Strongin, D.R., 2003. Pyrite oxidation inhibition by a cross-linked lipid coating. Geochem. Trans. 4 (2), 8.
Zhang, F., Zhao, L., Chen, H., Xu, S., Evans, D.G., Duan, X., 2008. Corrosion resistance of superhydrophobic layered double hydroxide films on aluminum. Angew. Chem. Int. Ed. 47 (13), 2466–2469.
Zhou, C., Lu, X., Xin, Z., Liu, J., 2013. Corrosion resistance of novel silane-functional polybenzoxazine coating on steel. Corros. Sci. 70, 145–151.
Zhu, D., van Ooij, W.J., 2003. Corrosion protection of AA 2024-T3 by bis-[3-(triethoxysilyl) propyl] tetrasulfide in sodium chloride solution. Part 2: mechanism for corrosion protection. Corros. Sci. 45 (10), 2177–2197.